JOURNAL OF AIRCRAFT
Vol. 44, No. 2, March–April 2007

Transonic Computational Fluid Dynamics Calculations on Preproduction F/A-18E for Stability and Control

Bradford E. Green* and James J. Chung*
NAVAIR, Patuxent River, Maryland 20670

DOI: 10.2514/1.22846

Computational fluid dynamics was used to predict the longitudinal and lateral/directional stability and control characteristics of an 8%-scale wind tunnel model of the preproduction F/A-18E Super Hornet at two transonic Mach numbers without any prior knowledge of existing wind tunnel or flight test data. The tetrahedral unstructured software system was used to generate and analyze grids during this computational study. The longitudinal stability and control characteristics of the aircraft were evaluated using three different horizontal tail deflections. Before evaluating nonzero horizontal tail deflections, coarse, medium and fine grids of the preproduction F/A-18E with a horizontal tail deflection of 0 deg were used in a grid resolution study to determine the grid density that was required to accurately calculate the forces and moments of the aircraft. The grid resolution study indicated that the medium grid was adequate at Mach 0.8 whereas the fine grid was necessary at Mach 0.9. The medium and fine grids with tail deflections of −6 and 6 deg were then generated and analyzed at Mach 0.8 and Mach 0.9, respectively, to determine the longitudinal stability and control characteristics of the aircraft. The lateral/directional stability and control characteristics of the preproduction F/A-18E were evaluated using a range of sideslip angles for several different angles of attack at Mach 0.8 and 0.9. The computational results compared very favorably to the existing wind tunnel data.

Nomenclature

C_A	=	aircraft axial force coefficient
C_D	=	aircraft drag coefficient
C_L	=	aircraft lift coefficient
C_l	=	aircraft rolling moment coefficient
C_m	=	aircraft pitching moment coefficient
C_N	=	aircraft normal force coefficient
C_n	=	aircraft yawing moment coefficient
C_Y	=	aircraft side force coefficient
Re_c	=	Reynolds number based on mean aerodynamic chord
α	=	angle of attack, deg
β	=	angle of sideslip, deg
δ_s	=	horizontal tail deflection angle, deg

I. Introduction

THE analysis of stability and control (S&C) characteristics of aircraft involves the analysis of behavior at and beyond the edge of the flight envelope. At these conditions, aerodynamic characteristics are difficult to predict due to massive flow separation, effects of aircraft dynamic motions, and time-dependent phenomena. Traditionally, wind tunnels have been used by the S&C community to analyze the characteristics of aircraft in this difficult flow regime. Wind tunnels, however, have limitations (Reynolds number, for example) and sometimes cannot accurately predict the aerodynamic characteristics of the aircraft. Although computational fluid dynamics (CFD) could be used to model the aircraft at flight conditions at the edge of the envelope, CFD has not yet been proved for these conditions. This research represents an initial exploratory investigation into using CFD for predicting the S&C characteristics of aircraft.

Because of the inherent difficulty in accurately predicting the S&C characteristics of the aircraft at the edge of the envelope, nearly every advanced aircraft program has been surprised by unpredicted, undesirable aerodynamic phenomena [1]. Eliminating these undesirable characteristics is both costly and time consuming, due to the amount of wind tunnel and "cut and try" flight testing involved. As a result, it is desirable to find and fix problems early in a program. Although CFD could be used in conjunction with wind tunnel tests to find potential problems, S&C engineers are not trusting of CFD due to the lack of applications and calibrations of the codes. CFD has been used with success to predict the aerodynamic performance of aircraft and for flow diagnostics, but CFD has not been widely used for force and moment calculations for S&C. This lack of trust of today's CFD codes by the S&C engineers creates a gap between CFD users and the S&C community.

As a result of the disconnect between CFD users and the S&C community, the National Aeronautics and Space Administration (NASA), with participation from the department of defense and industry, started the computational methods for stability and control (COMSAC) program. The COMSAC program was formed to improve the CFD tools for use in S&C applications and to bridge the gap between CFD and S&C. In September 2003 in Hampton, Virginia, the COMSAC program brought together over 100 CFD experts and S&C engineers from government and industry to share their present and future needs.

As a result of the COMSAC initiative, a project within the Common High Performance Computing Software Support Initiative (CHSSI) is dedicated to making improvements to CFD codes that would improve their ability to quickly and accurately predict the S&C characteristics of complex aircraft configurations. This project, named Integrated Simulation of Air Vehicle Performance, Stability and Control for Test and Evaluation, is within the Collaborative Simulation and Testing (CST) integrated portfolio. This project comprises engineers from Naval Air Systems Command (NAVAIR), NASA Langley, the Air Force Research Laboratory, and numerous contractors and consultants.

The present study is part of the CHSSI project. During this study, the longitudinal and lateral/directional S&C characteristics of the preproduction F/A-18E were evaluated using CFD. The preproduction F/A-18E was chosen as the baseline for this study

Presented as Paper 6122 at the Atmospheric Flight Mechanics, San Francisco, CA, 15–18 August 2005; received 30 January 2006; revision received 16 November 2006; accepted for publication 28 November 2006.

*Aerospace Engineer, Building 2187, Unit 5, Suite 1320-B, 48110 Shaw Road.

because of the complex, time-dependent nature of the flow over the aircraft at transonic speeds and the vast amount of wind tunnel data that exists for this aircraft.

During the engineering and manufacturing development (EMD) phase of the F/A-18E/F program, the F/A-18E experienced abrupt, uncommanded lateral activity during envelope expansion flights. This lateral activity was labeled as "wing drop" and a blue ribbon panel of experts was formed to investigate the phenomenon. The wing drop on the preproduction F/A-18E was caused by an abrupt, asymmetric change in the amount of flow separation on the wings. The asymmetric flow created a difference in the lift between the two wings, which caused the aircraft to abruptly roll. The wing drop on the preproduction aircraft was eliminated by modifying the leading-edge flap schedule and adding a porous surface over the wing-fold fairing. The production F/A-18E/F, which is being delivered to the fleet today, does not have wing drop.

As a result of the blue ribbon panel, the Abrupt Wing Stall (AWS) program [2] was formed to investigate wing drop and recommend ways by which future aircraft programs could predict and avoid it. The AWS program was composed of engineers from NASA Langley, NAVAIR, the Air Force and various universities, contractors, and consultants. The scope of the AWS program included extensive wind tunnel and CFD investigations. The preproduction F/A-18E was one of several aircraft that were investigated during this program.

The goal of the present study was to assess the ability of CFD to predict the longitudinal and lateral/directional S&C characteristics of the preproduction F/A-18E at transonic Mach numbers without prior knowledge of existing wind tunnel or flight test data. The accuracy of the CFD results in the wing-drop angle of attack (AOA) regime was of particular interest. Accomplishing this goal will help to bridge the gap between CFD users and S&C engineers. Specifically, successful completion of the study should impress upon S&C engineers the value of CFD to their real-world problems while simultaneously educating CFD users about the needs of the S&C community.

To accomplish the goal of this study, a grid refinement study was first performed using grids of the preproduction F/A-18E for three different fidelities. These grids, referred to as the coarse, medium, and fine grids, were analyzed by the flow solver USM3Dns at two transonic Mach numbers. The lift, drag, normal force, axial force, and pitching moment coefficients were compared between the grid solutions to determine the grid fidelity that was required at each Mach number to accurately predict the longitudinal S&C characteristics of the aircraft. The medium grid was found to be adequate at Mach 0.8, while the fine grid was determined to be necessary at Mach 0.9. The grid refinement study was conducted with a horizontal tail deflection of 0 deg.

Medium and fine grids were then generated with horizontal tail deflections of -6 and 6 deg to evaluate the impact of the deflections on the longitudinal S&C characteristics at Mach 0.8 and 0.9, respectively. The CFD calculations were performed without any prior knowledge of existing wind tunnel data. Once the CFD calculations were completed, the forces and moments from the CFD calculations were compared to the existing wind tunnel data.

After completing the longitudinal calculations, the lateral/directional S&C characteristics of the aircraft were predicted using CFD. Several sideslip angles were analyzed at select AOAs at Mach 0.8 and 0.9. The rolling moment, yawing moment, and side force coefficients from the CFD calculations were then compared to the existing wind tunnel data. The scope of this study included analyses of the accuracy of predicted stability characteristics (slope of moments with angle of attack and/or sideslip) and control effectiveness (magnitude of moment produced by controlled deflection).

In the following section, the grid generator and flow solver used during this study are discussed. A description of the geometry and grids is included in Sec. III. In Sec. IV, the computer requirements and solution convergence are discussed. The grid refinement study is then presented in Sec. V. A description of the wind tunnel data used for validation is discussed in Sec. VI. The results of the longitudinal and lateral/directional CFD predictions are shown in Secs. VII and VIII. Finally, some conclusions of the study are offered in Sec. IX.

II. Discussion of Grid Generator and Flow Solver

The Tetrahedral Unstructured Software System (TetrUSS) [3] was used to generate and analyze grids of the preproduction F/A-18E during this study. TetrUSS was developed at NASA Langley Research Center. This software system is capable of generating grids on complex configurations, analyzing the grids with a flow solver, and postprocessing the results. TetrUSS uses GridTool and VGRIDns to generate unstructured tetrahedral grids that can then be analyzed by the USM3Dns Navier–Stokes flow solver. Although not used during this study, TetrUSS also includes the ViGPLOT flow visualization program that can be used to postprocess the flow solutions generated by USM3Dns.

The grid generation process is begun using GridTool. In GridTool, a series of points and curves are used to form patches on the surface of the geometry. In addition, sources that control the size and density of the cells in the grid are created in GridTool. VGRIDns [4] then uses these patches and sources to generate an unstructured tetrahedral grid. VGRIDns uses the advancing-layers method to generate unstructured cells in the boundary layer and the advancing front method to generate cells in the inviscid region of the grid.

USM3Dns [5] is a three-dimensional, cell-centered, finite volume Navier–Stokes flow solver for unstructured, tetrahedral meshes. USM3Dns uses Roe's flux-difference splitting technique to compute the inviscid flux quantities across each cell face. The MinMod flux limiter was also implemented within USM3Dns for this study. The implicit Gauss–Seidel time-stepping scheme was used to advance the solution to a steady-state condition. Although only steady-state solutions were generated during this study, USM3Dns is capable of performing time-accurate calculations.

The one-equation turbulence model of Spalart–Allmaras [6] is available within USM3Dns in wall-function or full-viscous mode. Spalart–Allmaras is used to form a detached-eddy simulation (DES) for time-accurate calculations.

III. Geometry and Grid Descriptions

A. Geometry Description

The geometry evaluated during this computational study was that of the 8%-scale preproduction F/A-18E wind tunnel model. A picture of the computational geometry is shown in Fig. 1. The wing was modeled with 6/8/4 flaps, indicating that the leading-edge flap was deflected 6 deg, the trailing-edge flap was deflected 8 deg, and the aileron was deflected 4 deg downward. The geometry was modeled with both horizontal and vertical tails present. Horizontal tail deflections of -6, 0, and 6 deg were evaluated for the longitudinal study, while a horizontal tail deflection of 0 deg was used for the lateral/directional study. A Sidewinder missile and launcher were modeled at the wing tip and the inlet was modeled as flow-thru.

The aft-body distortion required for sting mounting of the 8%-scale wind tunnel model was included in the computational

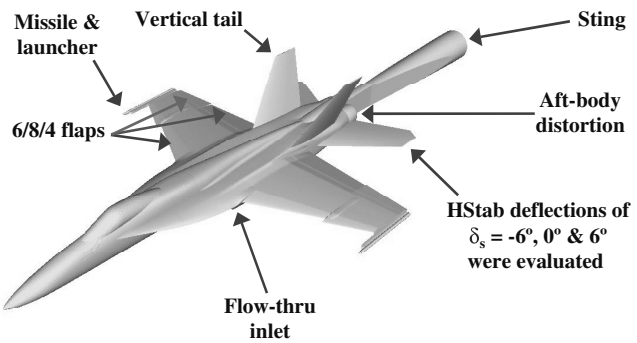

Fig. 1 The computational geometry of the 8%-scale wind tunnel model of the preproduction F/A-18E Super Hornet considered during this study.

geometry. In addition to the aft-body distortion, the sting was also included in the computational geometry. The sting geometry was truncated at 50% fuselage length behind the nozzle.

B. Grid Descriptions

Grids with four different fidelities were used during this study. Coarse, medium, and fine grids were used for the predictions of the longitudinal stability and control characteristics. In these three grids, only half of the aircraft was modeled and a symmetry-plane boundary condition was implemented. The fourth grid included the full aircraft and was used for the lateral/directional stability and control calculations.

All of the grids generated during this study had viscous tetrahedral cells near the surface and inviscid tetrahedral cells away from the surface. The *y*-plus value of the first cell above the surface was approximately unity for each of the grids.

1. *Coarse Grid*

The coarse grid, with 6.5×10^6 cells, was generated from a grid used during the AWS program where the flow on the wing was most important. As a result, the grid spacing was relatively coarse on the horizontal and vertical tails, causing concern that the coarse grid was inadequate for accurately predicting the longitudinal S&C characteristics of the aircraft. The coarse grid was generated with a horizontal tail deflection of 0 deg.

2. *Medium Grid*

The medium grid, with 11.5×10^6 cells, was generated with the intention of making the grid better suited for predicting the longitudinal S&C characteristics of the aircraft. The medium grid is shown in Fig. 2. The coarse grid was used as a starting point for generating the medium grid. In generating the medium grid, cells were added to the horizontal and vertical tails to eliminate the coarse grid size in that vicinity. The grids on the tails were made to be as fine as the grid on the wing in the hopes of capturing the impact of the tails on the pitching moment coefficient. Also in making the medium grid, the number of points in the boundary layer was increased over the entire aircraft. Pictures of the coarse and medium grids in the vicinity of the tails are shown in Fig. 3. Medium grids were generated with horizontal tail deflections of −6, 0, and 6 deg.

3. *Fine Grid*

The fine grid, with 15.1×10^6 cells, was developed from the medium grid by adding points to the wing, while leaving the grid elsewhere unchanged. Pictures of the medium and fine grids in the vicinity of the wing are shown in Fig. 4. Fine grids were generated with horizontal tail deflections of −6, 0, and 6 deg.

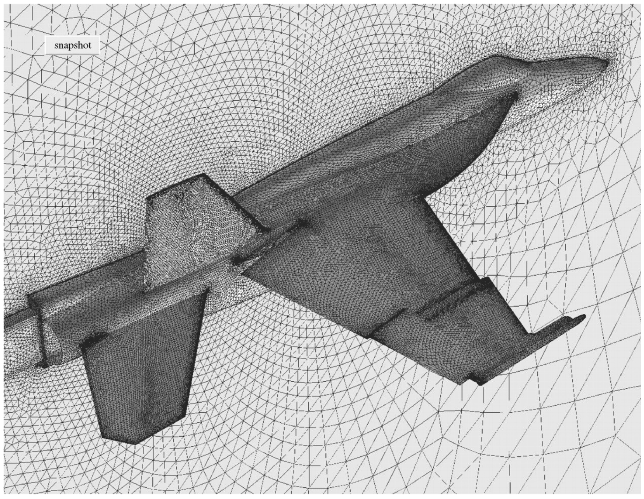

Fig. 2 The medium grid with 11.5×10^6 cells and a horizontal tail deflection of 0 deg.

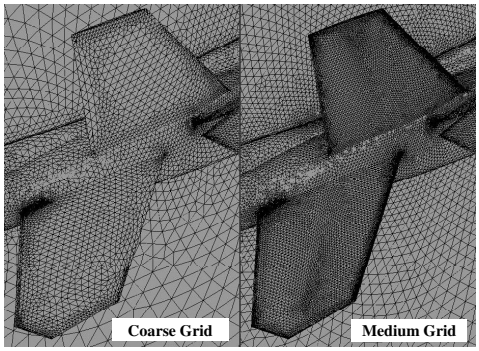

Fig. 3 The coarse and medium grids in the vicinity of the tails.

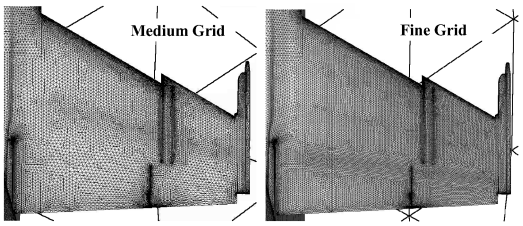

Fig. 4 The medium and fine grids in the vicinity of the wing.

4. *Lateral/Directional Grid*

The grid for the lateral/directional calculations contained 16.2×10^6 cells. In making this grid, the intent was to mirror the medium grid in the spanwise direction creating a grid with 23×10^6 cells. However, this desire was prohibited by computer memory limitations. Because concern existed that the coarse grid was inadequate for lateral/directional calculations, a new half-plane grid was generated with 8.1×10^6 cells. This grid represents a good compromise between the coarse and medium grids, and still has adequate grid fidelity on the horizontal and vertical tails. The new half-plane grid was then mirrored in the spanwise direction to generate a symmetric full-span grid for lateral/directional calculations. The lateral/directional grid was generated with a horizontal tail deflection of 0 deg.

IV. Computer Requirements and Solution Convergence

The calculations presented in this paper were performed on SGI Origin 3800/3900 machines available through the High Performance Computing Modernization Office (HPCMO). Each case was run using either 32 or 64 processors. Table 1 shows the computer time required for the grid resolution study, the longitudinal study, and the lateral/directional study. The total CPU time required for this project is less than the sum of the totals in Table 1, because some of the results from the grid resolution study were used for the longitudinal study.

Each solution was deemed "converged" when the total lift, drag, and pitching moment coefficients on the viscous surfaces did not change more than 0.0001 in 500 iterations. Reductions in residual of at least 3 orders of magnitude were typical.

V. Grid Resolution Study

Because the CFD calculations were to be performed without any prior knowledge of existing wind tunnel or flight test data, a grid

Table 1 Number of solutions and CPU requirements for the grid resolution, longitudinal and lateral/directional studies

Study	Number of solutions	CPU time, h
Grid resolution study	60	215,000
Longitudinal study	73	387,000
Lateral/directional study	30	135,000

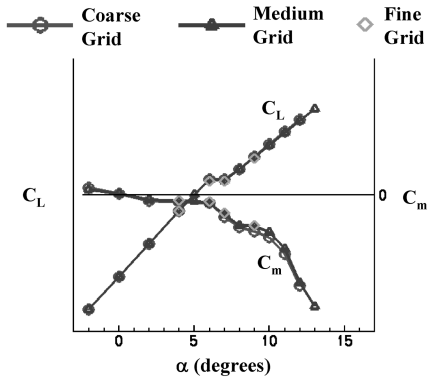

Fig. 5 The lift and pitching moment coefficients versus angle of attack for the coarse, medium, and fine grids at Mach 0.8 and $Re_c = 3.9 \times 10^6$ with 6/8/4 flaps and $\delta_s = 0$ deg.

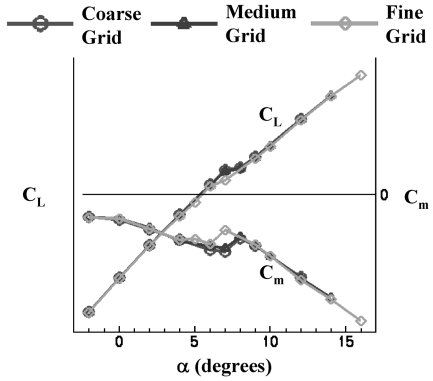

Fig. 6 The lift and pitching moment coefficients versus angle of attack for the coarse, medium, and fine grids at Mach 0.9 and $Re_c = 4.0 \times 10^6$ with 6/8/4 flaps and $\delta_s = 0$ deg.

resolution study was performed to determine the size of the grid necessary to accurately calculate the forces and moments on the preproduction F/A-18E. Accurately predicting the longitudinal characteristics of the aircraft was the main objective of performing the grid refinement study. In this section, the results of the grid refinement study at Mach 0.8 and 0.9 are presented.

A. Mach 0.8 Results

The lift and pitching moment coefficients are plotted as a function of AOA for the coarse, medium, and fine grids at Mach 0.8 and a tail deflection angle of 0 deg in Fig. 5 for $2 < \alpha < 12$ deg. Results for lift and pitching moment coefficients are nearly identical for the medium and fine grids. Although the coarse grid results are very similar to those of the medium and fine grid results, the pitching moment coefficient of the coarse grid near $\alpha = 10$ deg is slightly more negative than that of the medium and fine grids. Because horizontal tail deflections of −6 and 6 deg were going to be evaluated, it was anticipated that this difference in pitching moment could become larger for the nonzero tail deflections. As a result, the medium grid was used for the calculations with horizontal tail deflections of −6 and 6 deg at Mach 0.8. The sudden slope change in the lift and pitching moment curves in Fig. 5 at $\alpha = 6$ deg are indicative of the AWS phenomenon that the preproduction F/A-18E experienced.

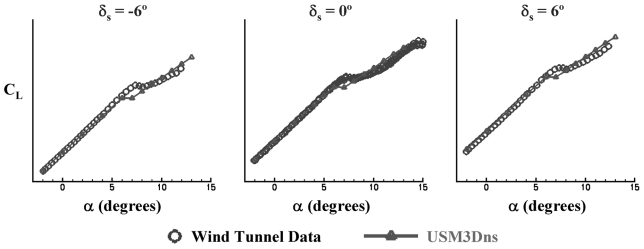

Fig. 7 The lift coefficient versus angle of attack for USM3Dns and the wind tunnel data at Mach 0.8 and $Re_c = 3.9 \times 10^6$ with 6/8/4 flaps and $\delta_s = -6$, 0, and 6 deg.

B. Mach 0.9 Results

The lift and pitching moment coefficients for the coarse, medium, and fine grids at Mach 0.9 and a tail deflection angle of 0 deg are shown in Fig. 6 for $2 < \alpha < 14$ deg. The lift and pitching moment coefficients for the coarse, medium, and fine grids are very similar. However, the onset of stall AOA for the fine grid is 1 deg lower than that for the coarse and medium grids. As a result, there is a significant difference in the lift and pitching moment coefficients at $\alpha = 7$ deg resulting in earlier instability (positive slope of pitching moment vs AOA curve).

Without prior knowledge of the wind tunnel data, it was assumed that the solutions generated with more points on the wing would be more accurate than those solutions with less resolution on the wing. Recall that the fine grid has more resolution on the wings than the coarse and medium grids. As a result, the fine grid was used to analyze the configurations with horizontal tail deflections of −6 and 6 deg at Mach 0.9.

VI. Description of Wind Tunnel Data

The wind tunnel data to which the CFD results were compared in this study were obtained at wind tunnels at NASA Langley Research Center in Hampton, Virginia, NASA Ames Research Center in Moffett Field, California, and CALSPAN in Buffalo, New York. The test number, facility, location, and tail configuration for each 8%-scale F/A-18E wind tunnel test are shown in Table 2. The two columns on the right side of the table indicate whether the data from the test were used to validate the longitudinal S&C calculations, the lateral/directional S&C calculations, or both.

VII. Longitudinal Stability and Control Predictions

A. Mach 0.8 Results

In Figs. 7–11, the CFD results are compared to the wind tunnel data for Mach 0.8, a Reynolds number of 3.9×10^6 based on a mean aerodynamic chord (MAC) and 6/8/4 flaps. Horizontal tail deflections of −6, 0, and 6 deg were evaluated and are shown in the plots.

The lift coefficients are compared in Fig. 7. The CFD results compare well with the wind tunnel data for $-2 < \alpha < 6$ deg. At $\alpha = 7$ deg, CFD underpredicts the lift coefficient and, as a result, the onset of stall predicted by CFD occurs earlier than the wind tunnel data indicates. For $8 < \alpha < 12$ deg, CFD predicts an approximately

Table 2 Details of the wind tunnel tests used for validation of the longitudinal and lateral/directional S&C CFD calculations performed during this study

Test no.	Facility	Location	Tail configuration	Used for long. study?	Used for lat./dir. study?
207	11-ft transonic tunnel	NASA Ames	$\delta_s = -6$, 0, and 6 deg	Yes	No
523	16-ft transonic tunnel	NASA Langley	$\delta_s = 0$ deg	Yes	Yes
565	16-ft transonic tunnel	NASA Langley	$\delta_s = 0$ deg	No	Yes
6149	8-ft transonic tunnel	CALSPAN	$\delta_s = 0$ deg	Yes	No
6151	8-ft transonic tunnel	CALSPAN	$\delta_s = 0$ deg	Yes	Yes

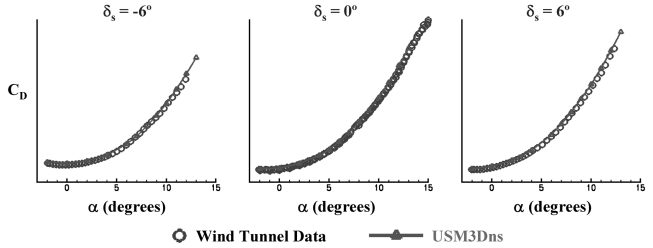

Fig. 8 The drag coefficient versus angle of attack for USM3Dns and the wind tunnel data at Mach 0.8 and $Re_c = 3.9 \times 10^6$ with 6/8/4 flaps and $\delta_s = -6$, 0, and 6 deg.

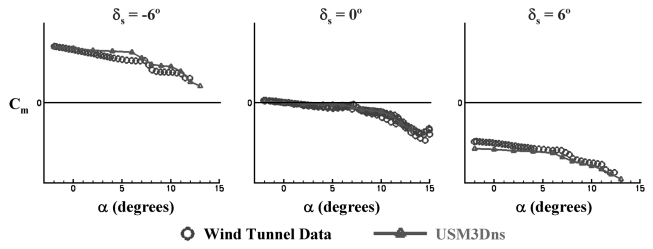

Fig. 9 The pitching moment coefficient versus angle of attack for USM3Dns and the wind tunnel data at Mach 0.8 and $Re_c = 3.9 \times 10^6$ with 6/8/4 flaps and $\delta_s = -6$, 0, and 6 deg.

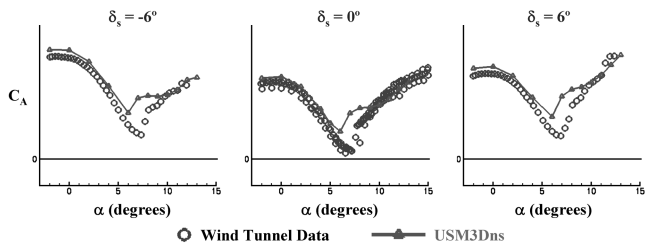

Fig. 10 The axial force coefficient versus angle of attack for USM3Dns and the wind tunnel data at Mach 0.8 and $Re_c = 3.9 \times 10^6$ with 6/8/4 flaps and $\delta_s = -6$, 0, and 6 deg.

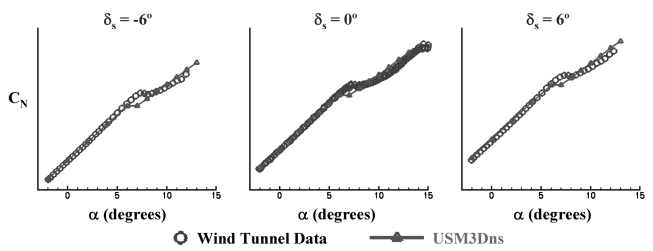

Fig. 11 The normal force coefficient versus angle of attack for USM3Dns and the wind tunnel data at Mach 0.8 and $Re_c = 3.9 \times 10^6$ with 6/8/4 flaps and $\delta_s = -6$, 0, and 6 deg.

linear variation of lift where the wind tunnel indicates otherwise. The reasons for these discrepancies are not known, but may be related to the unsteady nature of the AWS phenomena described earlier.

The drag coefficient for CFD and the wind tunnel is plotted in Fig. 8. As can be seen in this figure, the drag from USM3Dns compares very well with the wind tunnel data for the three tail deflections that were evaluated.

The pitching moment coefficient is plotted as a function of AOA for the three tail deflections in Fig. 9. For $\delta_s = 0$ deg, the CFD results lie within the spread of the wind tunnel data. At $\delta_s = -6$ and 6 deg, USM3Dns predicts less stable longitudinal stability characteristics for $-2 < \alpha < 6$ deg. However, CFD does properly predict the general magnitude of the pitching moment coefficient. Furthermore, CFD predicts slope changes in the pitching moment curves at $\alpha = 6$, 8, and 10 deg. These slope changes from CFD are predicted within 1 deg AOA of the slope changes shown in the wind tunnel data.

The axial force coefficient for CFD is compared to that of the wind tunnel data in Fig. 10. Although slightly overpredicted, CFD accurately predicts the axial force for $-2 < \alpha < 6$ deg. For $9 < \alpha < 12$ deg, the axial force from CFD compares well with the wind tunnel data. On the other hand, CFD significantly overpredicts the axial force of the wind tunnel data for $6 < \alpha < 9$ deg. CFD indicates an earlier break in axial force which is indicative of sudden loss of leading-edge suction, also associated with the abrupt stall characteristics of this configuration. Time-accurate DES methods may be necessary to accurately predict this region of the curve.

The normal force coefficient is plotted in Fig. 11 as a function of AOA. The normal force shows the same trend as the lift coefficient shown in Fig. 7.

In an effort to show the usefulness and accuracy of the CFD results obtained during this study, the stability derivatives from CFD were used to calculate the frequency and damping of the short-period mode of the preproduction F/A-18E flying at Mach 0.8 and 30,000 ft at $\alpha = 10$ deg. The same calculation was then performed using the stability derivatives from the wind tunnel data. The differences between the CFD and wind tunnel results for the frequency and damping were found to be insignificant.

B. Mach 0.9 Results

In Figs. 12–15, the CFD results are compared to the wind tunnel data for Mach 0.9, a Reynolds number of 4.0×10^6 based on MAC and 6/8/4 flaps for horizontal tail deflections of −6, 0, and 6 deg.

In Fig. 12, the lift coefficient is plotted as a function of AOA for the CFD results and the wind tunnel data. The lift predicted by CFD is fairly linear, while the wind tunnel data show a large slope change around $\alpha = 8$ deg. For $-2 < \alpha < 6$ deg, the CFD compares well to the wind tunnel data. Above $\alpha = 6$ deg, there are drastic differences between the CFD and wind tunnel results. These differences indicate the need for more analysis, including time-accurate calculations.

The drag coefficient is plotted versus AOA in Fig. 13. The drag coefficient from CFD compares very well to the wind tunnel data for all three tail deflections.

The pitching moment coefficient is plotted as a function of AOA for the CFD results and the wind tunnel data in Fig. 14. The magnitude of the pitching moment coefficient was accurately predicted by CFD for all three tail deflections, although the magnitude was slightly overpredicted for the horizontal tail deflection of 6 deg. CFD also did a good job of predicting the slope of the curves, although the slopes differ slightly around $\alpha = 6$ or 7 deg.

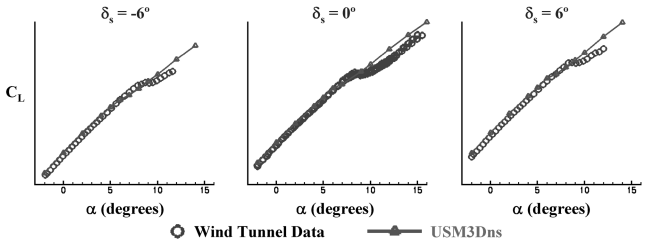

Fig. 12 The lift coefficient versus angle of attack for USM3Dns and the wind tunnel data at Mach 0.9 and $Re_c = 4.0 \times 10^6$ with 6/8/4 flaps and $\delta_s = -6$, 0, and 6 deg.

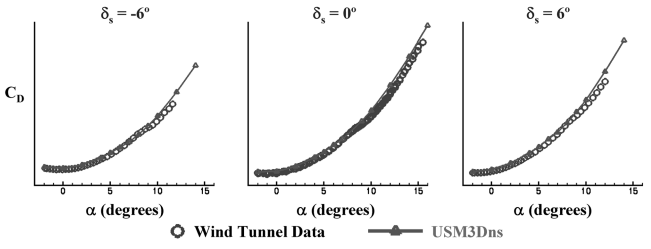

Fig. 13 The drag coefficient versus angle of attack for USM3Dns and the wind tunnel data at Mach 0.9 and $Re_c = 4.0 \times 10^6$ with 6/8/4 flaps and $\delta_s = -6$, 0, and 6 deg.

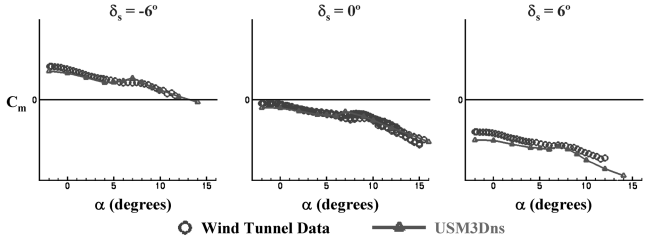

Fig. 14 The pitching moment coefficient versus angle of attack for USM3Dns and the wind tunnel data at Mach 0.9 and $Re_c = 4.0 \times 10^6$ with 6/8/4 flaps and $\delta_s = -6$, 0, and 6 deg.

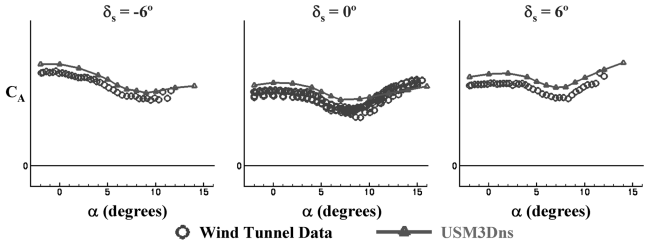

Fig. 15 The axial force coefficient versus angle of attack for USM3Dns and the wind tunnel data at Mach 0.9 and $Re_c = 4.0 \times 10^6$ with 6/8/4 flaps and $\delta_s = -6$, 0, and 6 deg.

The axial force coefficient is plotted in Fig. 15. Although CFD overpredicts the axial force coefficient, CFD did a great job of predicting the slopes of the curves. The normal force coefficient was not plotted, because the trend of the normal force coefficient is the same as that of the lift coefficient shown in Fig. 12.

VIII. Lateral/Directional Stability and Control Predictions

A. Mach 0.8 Results

In Figs. 16 and 17, the rolling moment, yawing moment, and side force coefficients for the CFD calculations and the wind tunnel data are plotted as a function of the sideslip angle for Mach 0.8, $\alpha = 5$ and 10 deg. Sideslip angles of -5, 0.1, and 5 deg were evaluated for the CFD calculations. From the figures, it can be seen that the comparison between the CFD calculations and the wind tunnel data is exceptional, indicating that USM3Dns provided very accurate predictions for this particular aircraft configuration.

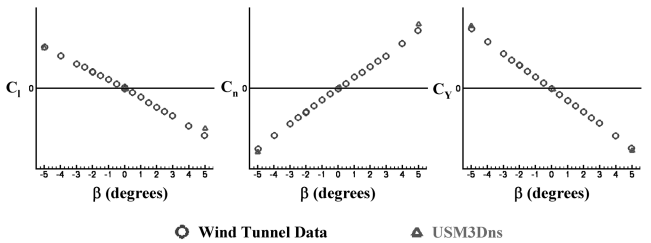

Fig. 16 The rolling moment, yawing moment, and side force coefficients versus sideslip angle for USM3Dns and the wind tunnel data at Mach 0.8, $Re_c = 3.9 \times 10^6$, $\alpha = 5$ deg with 6/8/4 flaps and $\delta_s = 0$ deg.

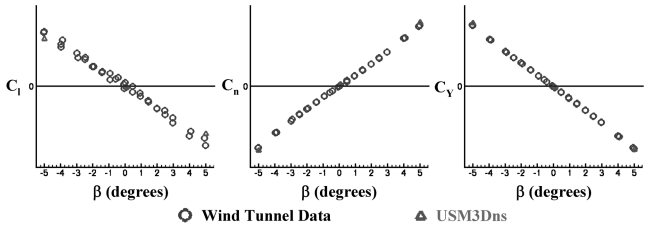

Fig. 17 The rolling moment, yawing moment, and side force coefficients versus sideslip angle for USM3Dns and the wind tunnel data at Mach 0.8, $Re_c = 3.9 \times 10^6$, $\alpha = 10$ deg with 6/8/4 flaps and $\delta_s = 0$ deg.

Using the stability derivatives obtained from the CFD calculations presented in this paper, the frequency and damping characteristics of the dutch roll mode of the preproduction F/A-18E were evaluated. The calculation was performed with the aircraft flying at Mach 0.8 and 30,000 ft at $\alpha = 10$ deg. The same calculation was then performed using the stability derivatives from the wind tunnel data. The differences between the CFD and the wind tunnel results for the frequency and damping were insignificant.

B. Mach 0.9 Results

At Mach 0.9, the lateral/directional characteristics were evaluated using CFD at $\alpha = 5$, 7, and 10 deg. More sideslip angles were evaluated at $\alpha = 7$ deg because AWS occurs in this regime and two different wind tunnel tests did not agree on the rolling moment characteristics at this AOA. A sideslip angle of 0.1 deg was evaluated rather than an angle of 0 deg in the hopes that any tendencies toward significant flow asymmetry could be initiated.

In Figs. 18–20, the rolling moment, yawing moment, and side force coefficients for the CFD calculations and the wind tunnel data are plotted as a function of the sideslip angle for Mach 0.9, $\alpha = 5$, 7, and 10 deg. For the most part, the CFD calculations compare very well with the wind tunnel data. The wind tunnel data shown in Fig. 19 for the $\alpha = 7$ deg case were taken from two different wind tunnels. The difference between the rolling moment coefficients from the two wind tunnels is very evident.

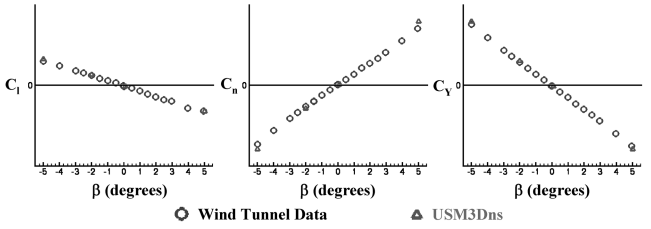

Fig. 18 The rolling moment, yawing moment, and side force coefficients versus sideslip angle for USM3Dns and the wind tunnel data at Mach 0.9, $Re_c = 4.0 \times 10^6$, $\alpha = 5$ deg with 6/8/4 flaps and $\delta_s = 0$ deg.

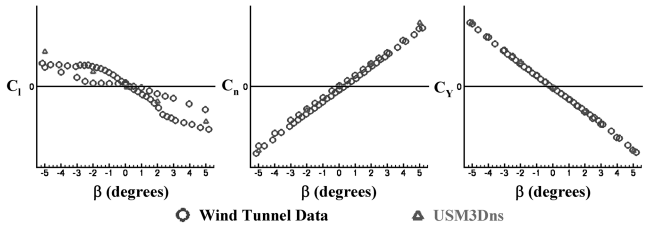

Fig. 19 The rolling moment, yawing moment, and side force coefficients versus sideslip angle for USM3Dns and the wind tunnel data at Mach 0.9, $Re_c = 4.0 \times 10^6$, $\alpha = 7$ deg with 6/8/4 flaps and $\delta_s = 0$ deg.

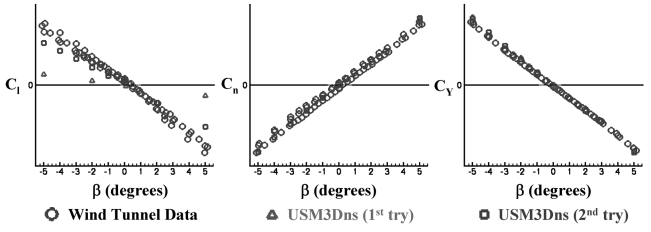

Fig. 20 The rolling moment, yawing moment, and side force coefficients versus sideslip angle for USM3Dns and the wind tunnel data at Mach 0.9, $Re_c = 4.0 \times 10^6$, $\alpha = 10$ deg with 6/8/4 flaps and $\delta_s = 0$ deg.

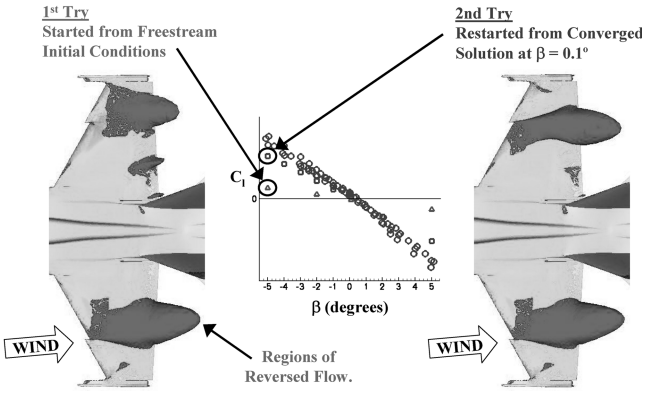

Fig. 21 Comparison between the rolling moment coefficient and the flow on the wing for two solution techniques at Mach 0.9, $Re_c = 4.0 \times 10^6$, $\alpha = 10$ deg, $\beta = -5$ deg with 6/8/4 flaps and $\delta_s = 0$ deg.

The rolling moment, yawing moment, and side force coefficients for Mach 0.9, $\alpha = 10$ deg are plotted in Fig. 20 as a function of the sideslip angle. In this figure, the results of two different USM3Dns calculations are shown. The triangular symbols represent the results of USM3Dns when the CFD calculations were started from freestream initial conditions. This is the same methodology that was used for all previous CFD results presented in this paper. In generating the results shown by the square symbols, the converged solution for the $\beta = 0.1$ deg case was used as the initial condition for each of the sideslip angles shown in Fig. 20. Although the yawing moment and side force are relatively independent of the initial condition, an improved correlation with the rolling moment coefficient was obtained when the converged $\beta = 0.1$ deg case was used as the initial condition. The data shown by the triangular symbols in Fig. 20 were generated without prior knowledge of the wind tunnel data. The subsequent CFD calculations shown by the square symbols were performed after seeing the poor correlation between the triangular symbols and the wind tunnel data.

As might be expected, the dramatic changes in the rolling moment coefficient at sideslip between CFD and experiment would be expected to be illustrated between the relative flowfields between the cases. The difference in the flow on the wings between the two different solution techniques for the $\beta = -5$ deg case is shown in Fig. 21. This figure shows the pressure coefficients and regions of reversed flow on the upper surface of the wings for the two different approaches. The illustration on the left side of the figure shows the results of the case that was started from freestream initial conditions, while the illustration on the right shows the results of the case that was started from the $\beta = 0.1$ deg converged solution. When one compares the regions of reversed flow between the two solutions, it can be seen that there is a drastic difference in the flow structure on the right wing. The fact that the flow on the right wing is dependent upon the initial conditions of the solution is indicative of the unsteady nature of the transonic flow over the F/A-18E/F. The unsteady nature of the flow over the F/A-18E/F at these conditions is well documented [7–9].

IX. Conclusions

This investigation was an exploratory use of an existing CFD code to predict the complex longitudinal and lateral/directional characteristics of the preproduction F/A-18E at transonic speeds. The flow on the F/A-18E at transonic speeds is massively separated and unsteady. Nonetheless, the correlation of CFD with the wind tunnel data is generally very good. More work is required to analyze differences apparently due to the effects of unsteadiness near wing stall. The agreement between the CFD results and the wind tunnel data for the longitudinal stability and control characteristics was good, although the agreement near wing stall was poor. The general character of the longitudinal control effectiveness was predicted reasonably well by the code. For the most part, CFD did an exceptional job of predicting the lateral/directional stability and control characteristics of the aircraft. At wing stall, large differences existed between two wind tunnels as well as CFD. Above wing stall at Mach 0.9, the CFD results were dependent upon the initial condition of the calculation because of the unsteady nature of the flow. Redoing the calculations with different initial conditions resulted in good agreement between the wind tunnel and CFD.

Based on the results of the present exploratory investigation, considerable promise exists for the application of CFD methods for future high performance aircraft. Such applications would allow the designer to augment his existing toolbox to extrapolate experimental predictions to higher values of Reynolds number, provide flow diagnostic capability for stability and control problems, and provide analysis capabilities where wind tunnel techniques are not available. Additional requirements for stability and control analysis such as aircraft dynamic motion effects on aerodynamics might be particularly fruitful areas of research in the near future. More calibrations of CFD for other airplane configurations will be required to convince stability and control engineers that CFD is a viable predictive tool.

Acknowledgments

The authors would like to gratefully acknowledge the funding that was granted for this study by the High Performance Computing Modernization Office (HPCMO) through the Common High Performance Computing Software Support Initiative (CHSSI) program. In addition, the authors would like to thank David Findlay, the point of contact for the Collaborative Simulation and Testing (CST) portfolio, for his guidance and insight. Also, the authors would like to thank the HPCMO for the many hours of computer time that was necessary to complete this computational study. Finally, the authors would like to acknowledge the following individuals for their advice and guidance: Steve Hynes and Alex Kokolios of Naval Air Systems Command (NAVAIR), Robert Hall, Neal Frink, and Mike Fremaux of NASA Langley, Joseph Chambers, retired NASA Langley and consultant, and Mohagna Pandya of Swales Aerospace.

References

[1] Chambers, J. R., and Hall, R. M., "Historical Review of Uncommanded Lateral-Directional Motions at Transonic Conditions," *Journal of Aircraft*, Vol. 41, No. 3, 2004, pp. 436–447; also AIAA Paper 2003-0590, Jan. 2003.

[2] Hall, R. M., and Woodson, S. H., "Introduction to the Abrupt Wing Stall Program," *Journal of Aircraft*, Vol. 41, No. 3, 2004, pp. 425–435; also AIAA Paper 2003-0589, Jan. 2003.

[3] Frink, N. T., Pirzadeh, S., Parikh, P., Pandya, M. J., and Bhat, M. K., "The NASA Tetrahedral Unstructured Software System (TetrUSS)," *The Aeronautical Journal*, Vol. 104, No. 1040, 2000, pp. 491–499.

[4] Pirzadeh, S., "Three-Dimensional Unstructured Viscous Grids by the Advancing Layers Method," *AIAA Journal*, Vol. 34, No. 1, 1996, pp. 43–49.

[5] Frink, N. T., "Tetrahedral Unstructured Navier-Stokes Method for Turbulent Flows," *AIAA Journal*, Vol. 36, No. 11, 1998, pp. 1975–1982.

[6] Spalart, P. R., and Allmaras, S. R., "A One-Equation Turbulence Model for Aerodynamic Flows," AIAA Paper 97-0644, Jan. 1997.

[7] Schuster, D. M., and Byrd, J. E., "Transonic Unsteady Aerodynamics of the F/A-18E Under Conditions Promoting Abrupt Wing Stall," *Journal of Aircraft*, Vol. 41, No. 3, 2004, pp. 485–492; also AIAA Paper 2003-0593, Jan. 2003.

[8] Forsythe, J. R., and Woodson, S. H., "Unsteady Computations of Abrupt Wing Stall Using Detached-Eddy Simulation," *Journal of Aircraft*, Vol. 42, No. 3, 2005, pp. 606–616; also AIAA Paper 2003-0594, Jan. 2003.

[9] Forsythe, J. R., Fremaux, C. M., and Hall, R. M., "Calculation of Static and Dynamic Stability Derivatives of the F/A-18E in Abrupt Wing Stall Using RANS and DES," *Proceedings of the 3rd International Conference on CFD*, July 2004.